Validation of a Miniaturized Permeability Assay Compatible with CRISPR-Mediated Genome-Wide Screen

by
Claire Simonneau[1§], Junning Yang[1], Xianguo Kong[1], Robert Kilker[1], Leonard Edelstein[1], Paolo Fortina[2], Eric Londin[3], and Arie Horowitz[*]

1 – Cardeza Center for Hematology Research, 2 – Department of Cancer Biology, 4 – Sidney Kimmel Cancer Center Genomics Laboratory, 3 – Computational Medicine Center, Sidney Kimmel Medical College, Thomas Jefferson University, Philadelphia, Pennsylvania, USA.

* – Corresponding author
§ – Current address: Roche Innovation Center Basel, Switzerland

Corresponding author: Arie Horowitz; email address: arie2006@gmail.com; telephone +1-617-784-2927

ABSTRACT

The impermeability of luminal endothelial cell monolayer is crucial for the normal function of the vascular and lymphatic systems. Its key is intercellular junction integrity. The known repertoire of junction-regulating genes is incomplete. Current permeability assays are incompatible with high-throughput genome-wide screens that could identify these genes. To overcome this limitation, we designed a new permeability assay that consists of cell monolayers grown on ~150 μm microcarriers. Each microcarrier functions as a miniature individual assay of permeability (MAP). We demonstrate that false-positive results can be minimized, and that MAP sensitivity to gene repression is similar to the sensitivity of the measurement of monolayer impedance. In this study, we validated the assay by showing that the expression of single guide RNAs (sgRNAs) that target genes coding known thrombin signaling proteins blocks effectively thrombin-induced junction disassembly, and that MAPs carrying such cells can be separated from those that carry cells expressing non-targeting sgRNAs by a fluorescent probe.

Keywords: cell junction, disassembly, fluorescent probe, thrombin, protease-activated receptor

INTRODUCTION

One of the new opportunities afforded by the sequencing of the human genome, as well as of many others, is the ability to run genome-wide reverse screens to identify genes that underlie diverse phenotypes. The repurposing of CRISPR/deactivated (d) Cas9 for targeting either repressive or activating modules to genomic loci provides a more versatile and specific tool than RNAi, becoming the screen method of choice [1]. In the few short years since this tool became available, it has already been applied to numerous ends, including cancer drug discovery [2], analysis of unfolded protein response [3], and the identification of cancer immunotherapy targets [4]. CRISPR/dCas9-mediated screens take advantage of the accurate sgRNA-dependent targeting of protein modules that either repress or activate transcription to proximal upstream and downstream regions near the transcription start site. Transcriptional activation has been achieved by various combinations of a range of modules, including NF-κB trans-activating subunit p65 [5], tetrameric VP16 transactivation domain (VP64), heat shock factor 1, the catalytic histone acetyltransferase core domain of the human E1A-associated protein p300, and the viral replication and transcription activator [reviewed in [6]]. In contrast, transcriptional repression has been produced by a single module, the Krüppel-associated box (KRAB) domain of the zinc-finger transcription factor Kox [7]. The efficacy of the regulatory dCas9-fused module is highly dependent on the selection of the sgRNA genomic targets relative to the transcription start sites, based on rules that were derived and optimized empirically [5, 8]. Activation on the order of 10^3-fold, as measured by quantifying mRNA levels of selected genes, was achieved by some of the above complexes [6], whereas transcriptional repression measured in the same way was on the order of 10^2-fold, and rarely 10^3-fold [9].

Genome-wide screens employing activating or repressive dCas9 constructs and sgRNA libraries were deployed to identify toxin or drug resistance and vulnerability-conferring genes [9-14], genes that mediate cell immune and inflammatory responses [15-18], and genes required for cell survival, proliferation, and metastasis [10, 19-22]. The majority of screens performed to date phenotyped cell enrichment or depletion, though some studies measured the rates of differentiation [23], cell motility [24], and the abundance of fluorescent protein [25]. In all cases, the quantified phenotypes were individual-cell attribute. Such assays are suitable to the pooled format that, with rare exceptions [26, 27], characterizes the vast majority of currently available sgRNA libraries, and enables a relatively facile and economical quantification of the phenotype. Though effective and fruitful, the current limitation to individual-cell functional assays leaves out collective cell functions which underlie physiologically essential processes. Here we validate a new functional assay we designed to facilitate adaptation of the CRISPR-mediated screen for the identification of genes that regulate the permeability of endothelial cell (EC) monolayers. The integrity of this monolayer is critical to the normal function of the vascular system because it confers the barrier function of the vessels. Because administration of thrombin produces large gaps in EC monolayers that can be detected with relative ease, we chose to validate the assay by testing if sgRNAs from an existing repressive CRISPR library [8] designed to knockdown the transcription of thrombin signaling pathway genes are enriched in cells that do not respond to it. Thrombin-induced permeability is not manifest in vertebrates under normal conditions, but does occur under trauma, sepsis, and other inflammation-inducing conditions in both animal models [28-30] and patients [31, 32].

Currently available permeability assays are not compatible with the requirement of genome-wide screens because they cannot accommodate the large number of samples, and because their multi-well format is unsuitable for the pooled sgRNA libraries used in practically all screens. To our knowledge, the highest sampling capacity currently available for the measurement of paracellular permeability is provided by the 96-well plate filter insert assay format. A comprehensive screen of the human genome by 10 sgRNAs and 5 technical replicates per gene

using this assay would require approximately 10^4 multi-well plates, a number that is beyond the capacity of most research laboratories. To design a more suitable assay, we took advantage of the microcarrier-based cell culture technique developed to maximize the number of adherent cells grown per volume of medium. Typically, microcarriers consist of spherical beads of a diameter in the range of 100-200 μm, made of cross-linked polymers. Commercially available microcarriers come in a variety of polymeric matrices and surface treatments or coatings [33]. Microcarriers carrying EC monolayers had been used to study the effect of various agonists on cell monolayer permeability by measuring the absorbance of dye into the microcarriers, or in a chromatographic format, by measuring the elution time of a dye [34-37]

RESULTS

EC monolayers grown on single microcarriers serve as individual permeability assays

We sought an in vitro permeability assay that would be compatible with the high throughput format required for genome-wide screens to interrogate signaling pathways that regulate the integrity of endothelial cell junctions. In contrast to the previous adaptation of microcarriers for measuring monolayer permeability, we consider each microcarrier as an individual MAP. This facilitates high throughput testing of a large number of samples in a relatively small volume of growth medium (approximately 4.3×10^5 microcarriers per 100 mL). We envisioned that ECs will be transduced by either repressive (CRISPRi) or activating (CRISPRa) sgRNA libraries and grown as clonal populations on each microcarrier. When treated by agonists that disrupt cell junctions, e.g. vascular endothelial growth factor (VEGF) or thrombin, junctions among ECs expressing sgRNAs that target genes required the for the cellular response to the administered agonist will fail to disassemble. To distinguish between microcarriers carrying responsive or non-responsive EC monolayers, we selected a probe that would bind to the microcarriers surface exposed through the gaps between the responsive cells. Since the microcarriers type that supported EC growth optimally is coated with gelatin, we selected the collagen-binding fragment of fibronectin (FN_c) [38] because of its high binding affinity to gelatin [39] and conjugated it to a fluorophore. MAPs carrying responsive EC monolayers would become fluorescent because of the binding of the fluorescently-conjugated fibronectin fragment to the newly formed gaps between ECs. These MAPs would then be separated from those carrying non-responsive monolayers by fluorescence-assisted sorting (Fig. 1).

Thrombin increases the permeability of telomerase-immortalized human primary EC monolayers

Among a variety of known permeability factors, we noted that thrombin induces relatively large openings between confluent ECs [40], as observed also when cells were grown on the same type of microcarriers used in this study [35]. We chose it, therefore, as a convenient agonist for testing MAP validity. To gauge thrombin's effects on the monolayers of the telomerase-immortalized human dermal microvascular ECs (TIME cells) we used throughout this study, we measured thrombin-induced change in permeability by two approaches. In the first, we measured the penetration of a fluorescently-conjugated dextran probe through an EC monolayer. In the second, we measured the thrombin-induced change in the impedance of the monolayer. Both approaches yielded large changes in the measured attributes, indicating substantial increases in monolayer permeability. In the first type of assay, where the measured leakage of the probe is a direct reflection of the formation of pores in the formerly confluent EC monolayer, the fluorescence of the probe in the lower chamber of the assay almost plateaued after a more than 3-fold increase (Fig. 2A). In impedance measurements, thrombin concentrations of 0.5, 1.0, and 2.0 U/mL reduced the impedance by approximately 1.1 units, although their rate of recovery to the pre-thrombin level became slower when thrombin concentration was increased (Fig. 2B). The impedances recovered their pre-thrombin levels and stabilized in approximately 120 min. To visualize the structural effects of thrombin on the EC

monolayer, we immunolabeled the cells to track the localization of vascular endothelial cadherin (VEcad) and used phalloidin to observe thrombin-induced changes in the actin cytoskeleton. Thrombin induced the opening of large gaps, which were in some locations as large as EC width (approximately 30 μm), and the formation of denser and thicker stress fibers (Fig. 2C), similar to previous observations [41].

Single TIME cells grow to confluence on gelatin-coated microcarriers

Following tests with several types of microcarrier polymers (e.g. polystyrene, diethylaminoethyl dextran), and coatings (e.g. fibronectin, collagen I), we determined that microcarriers consisting of cross-linked dextran matrix and coated with gelatin are optimal for TIME cell growth. To observe monolayer integrity, we stained them with calcein, a dye that visualized both the cell body and intercellular junctions (Fig. 3A). All the cells grown on each microcarrier in a genome-wide screen are required to express a single sgRNA to avoid mixed effects of silencing the expression of potentially antagonistic genes or additive effects of potentially cooperative genes. Consequently, the TIME cell monolayer on each microcarrier has to evolve from a single cell and form a clonal population. To achieve a 1:1 cell-microcarrier ratio, we used a seeded ratio of one cell per two microcarriers. Starting from a single cell, TIME cells reached confluence in nine days, forming tightly sealed monolayers similar cells grown from an initially larger number (Fig. 3B).

TIME cells grown on microcarriers form intact tight and adherens junctions

Formation of a cobblestone monolayer with integral intercellular junctions is essential for the repurposing of cell-coated microcarriers as individual permeability assays. Evidence for the establishment of such monolayers on the same type of microcarriers used here, including at the ultrastructural level, had been reported approximately 30 years ago [35, 42]. Furthermore, there is no apparent cause that would render formation of intact intercellular junctions less likely on a convex than on a flat surface. Nevertheless, we sought to show that junction-specific proteins are present at the junction of the specific cell type used in this study, as an indication of intercellular junction integrity. Tight junctions form a more restrictive barrier than adherens junctions, and do not permit the passage of proteins because of their size-selectivity [43]. To test their integrity, we immunolabeled JAM-A, a single-pass transmembrane protein, and the adaptor protein ZO1, which bind each other at tight junctions [44]. Both proteins were abundantly present at cell borders among all the cells that were visible in the field of view. They appeared as narrow undisrupted bands (Fig. 3C). The adherens junction marker vascular endothelial (VE)-cadherin was similarly patterned and abundant (ibid.). We conclude that the intercellular junctions formed by MAPs do not differ from junctions formed by the same (Fig. 2C) or other [45] ECs on flat surfaces.

Thrombin increases attachment of FN_c to gelatin-coated surfaces

To assess the compatibility of fluorophore-conjugated FN_c (FN_{cf}; Appendix SI, Fig. S1A), we tested if the extent of its binding to a gelatin-coated substrate depends on EC confluence. The fluorescence signal of the surface-attached probe on microcarriers carrying a confluent TIME cell monolayer was miniscule in comparison to the signal of sub-confluent monolayer (Appendix SI, Fig. S1B). Thrombin treatment of confluent TIME cell layers generated substantial gaps among adjacent cells (Appendix SI, Fig. S1C). Bare, gelatin-coated microcarriers bound FN_{cf} avidly, whereas microcarriers coated by a sub-confluent EC monolayer bound only a fraction of the latter (Appendix SI, Fig. S1D).

Likelihood of false discovery is reduced by removal of non-confluent microcarriers

Though the majority of TIME cell monolayers reached confluence even when grown from a single cell per microcarrier (Fig. 3B), it is practically impossible to ensure that the surface of all

microcarriers is fully coated by cells. Elimination of microcarriers that have residual exposed surface patches is essential because the FN_{cf} probe would bind to the exposed surface, resulting in the misidentification of the cells as intransigent to the sgRNA they were transduced with during a genome-wide screen. Such an error would result in the omission of potentially relevant genes. To eliminate sub-confluent microcarriers from the population, we sorted MAPs that were incubated with FN_{cf} in the absence of an agonist. Extinction profiles of individual MAPs peaked at the edges, likely corresponding to the gelatin and TIME cell layers (Fig. 4A). The fluorescence signal was frequently uniform across the imaged face of the microcarriers. Initially, we gated the MAP population to exclude debris or clusters of more than one MAP (Fig. 4B). The residual population was gated again to remove MAPs whose peak fluorescence intensity was at least two-fold higher than the intensity of the highest counts (ibid.). This subgroup, which we assumed would include the majority on non-confluent MAPs, amounted to 12 percent of the MAP population. To test the efficacy of this approach and the stability of cell monolayers on the MAPs during sorting, we scanned the sorted MAP population. The spreads of its extinction values and sizes were confined within a relative narrow range (Fig. 4C). A histogram of MAP peak fluorescence intensity revealed a similarly confined group, as expected (ibid.). Visual inspection of samples from the initial and residual populations confirmed the presence of exceptionally bright MAPs in the former (Fig. 4D), but not in the latter (Fig. 4E).

Fluorescence-assisted sorting separates MAPs carrying thrombin-treated and untreated TIME cells

Execution of a genome-wide screen requires physical separation between the phenotypes that ensue during the functional assay – in the current study, these are thrombin-responsive and non-responsive MAPs. The conjugation of FN_c to a fluorophore would enable separation by fluorescence-assisted sorting (FACS), albeit not by conventional instruments designed to handle cell-sized particles. In order to test the sensitivity of the sorter to the signal of junction disassembly detected by the binding of the FN_{cf} probe, after the assay was completed we fixed the microcarrier-attached TIME cells by EtOH, which is an optimal fixative for the preservation of nucleic acids [46]. Fixation prevented changes in cell and junction morphology. We then subjected the whole microcarrier population to fluorescence-assisted sorting on a FACS apparatus equipped with large-bore nozzle to accommodate the flow of MAPs. When using sgRNAs from a CRISPRi library, as in this study, the target population are MAPs that carry cells which did not respond to thrombin, presumably due to the repressive effect of the tested sgRNAs. These would be the microcarriers that emit the lowest fluorescence intensity during sorting, some of which would be detectable only by their extinction signal, because their fluorescence emission could be lower than the sensitivity of the sorter's light detector. Due to potential disparity in cell response to thrombin, among other conceivable biological variables, the light-intensity distribution of among the sorted MAP population was continuous over an interval between high and low intensity values, rather than binary. To produced two distinct sorted populations, we defined two gates, one for the low-responding microcarriers, referred to as 'negative', and the high-responders that we refer to as 'positive'. The percentage of the population of microcarriers that were not treated by thrombin and counted as negative fell from approximately 40 percent to only 10 percent of the thrombin-treated microcarrier population (Appendix SI, Fig. S2A), because of the upward shift in MAP fluorescence intensity. Complementarily, the percentage of positive microcarriers increased from approximately 15 to 40 percent of the treated microcarrier population (Appendix SI, Fig. S2B). These measurements demonstrate a robust and reproducible response to thrombin that can be readily resolved into positive and negative populations. A portion of approximately 45 percent of the total microcarrier population encompassing the medium of the response range remained between the upper and lower gates. This sub-population is least likely to contain microcarriers carrying cells that express the most repressive sgRNAs. Sidestepping this population was not likely, therefore, to

preclude the identification of genes that have major roles in mediating the disassembly of cell junctions in response to thrombin.

sgRNAs repress target gene expression level, protein abundance, and response to thrombin

To effectively test if the microcarrier-based permeability assay can achieve this separation by distinguishing between genes that affect EC response to thrombin, we selected sgRNAs that target *F2R*, the gene that encodes the main thrombin receptor in ECs [47], proteinase-activated receptor (PAR) 1, as a positive control. We chose *KDR*, the gene that encodes VEGF receptor 2, the main VEGF receptor in blood vessel ECs [48], as a negative control. We included sgRNAs that target *GNAQ*, a gene encoding $G\alpha_q$, a trimeric GTPase. $G\alpha_q$ mobilizes calcium by activating phospholipase C-β, but unlike $G\alpha_{11/12}$, it is not known to affect EC monolayer permeability [49]. We selected it, therefore, as an unknown whose effect on the permeability of microcarrier-attached TIME cell monolayers remains to be tested. Before testing the effects of the selected sgRNAs on EC barrier function, we validated the presumed capacity of each of the five individual sgRNAs designed to target single genes [8] by measuring how effectively they repressed the transcription of their target genes and, consequently, reduced the abundance of the protein these genes encode. Using quantitative real-time polymerase chain reaction (qRT-PCR), we detected a large variability among the repressive effects of each set of five sgRNAs that reached more than 13-fold in the case of *F2R*-targeting sgRNAs (Fig. 5A). The most effective one among the five sgRNAs repressed *F2R* transcription to approximately 6 percent of its expression level in TIME cells treated by non-targeting sgRNAs (ibid.). Based on immunoblotting, the pattern of PAR1 abundance in each cell group expressing a single sgRNA fit precisely the qRT-PCR expression pattern of *F2R,* which encodes PAR1. The single sgRNA-specific expression levels of *GNAQ* and *KDR* fit similarly well the abundances of $G\alpha_q$ and *KDR* (Fig. 5B, 5C), confirming that three to four sgRNAs out of each set of five were capable of repressing their target gene by at least 70 percent.

Efficient repression of *F2R* is expected to diminish the effect of thrombin on endothelial cell junctions, which typically lose their interconnections and retract, producing large intercellular gaps (Appendix SI, Fig. S1C). The effect of *GNAQ* repression, on the other hand, remained to be revealed in the planned permeability assays. To test these predictions, we measured the impedance before and after the application of thrombin of TIME cell populations expressing each of the most repressive sgRNAs of *F2R*, *GNAQ*, and *KDR*, grown in multi-well plates. The impedance of TIME cells expressing sgRNAs for *GNAQ*, *KDR*, and a validated negative-control (NC) sgRNA [8] fell by close to an impedance unit (Fig. 5D). The impedance of TIME cells expressing *F2R* sgRNA, on the other hand, fell only by 0.2 units and returned to the basal level earlier than the other cell groups.

MAP sensitivity to *F2R* knockdown is similar to impedance measurement

Insufficient sensitivity of a permeability assay may limit its utility in general and its capacity to detect genes that modify the response to the tested agonist in particular. We chose impedance measurement as a benchmark for assay sensitivity because this technique is more sensitive than that of cell monolayers cultured on a permeable substrate [50], the main alternative technique. We tested the sensitivity of impedance measurement as a detector of sgRNA-mediated knockdown of an essential gene by comparing the thrombin response of TIME cells transduced by the most effective *F2R*-targeting sgRNA, *F2R*-2, to cells transduced by a negative-control sgRNA. Whereas the impedance of cells transduced by the latter sgRNA fell by four units, the impedance of TIME cells transduced by *F2R*-2 fell only by 0.75 unit (Fig. 6A). As a first step in the test of MAP sensitivity to *F2R* knockdown, we repeated the procedure described above for the removal of particles that were not whole single MAPs and of non-

confluent single MAPs (Fig. 6B). The mean peak fluorescence intensity of thrombin-treated MAPs carrying cells transduced by the most effective *F2R*-targeting sgRNA was higher by approximately 18 percent than that of the same type of untreated MAPs (Fig. 6C). On the other hand, MAPs carrying cells transduced by a mixture of three negative control sgRNAs responded to thrombin by a four-fold increase in mean fluorescence intensity compared to an untreated group (Fig. 6D). To serve as a functional assay in a screen with a repressive sgRNA library, the technique is required to distinguish between MAPs that respond normally to the agonist, i.e. those that express sgRNAs irrelevant to the screened signaling pathway, and between repressive sgRNAs. We used a ratiometric approach to express this attribute as a dimensionless quantity that can reflect the sensitivities of dissimilar techniques that use incomparable units of measurements. We defined the sensitivity of the assay as the ratio between the response of cells which express an irrelevant sgRNA to the response of cells that express a repressive sgRNA. In this study, the two groups were represented by cells that express a mixture of three negative control sgRNAs versus those that express *F2R*-2. Thus, the sensitivity of the impedance measurement was calculated by the ratio between I_{NC} and I_{F2R} (Fig. 6A), whereas MAP sensitivity was calculated by the ratio between $F_{NCT}–F_{NCU}$ (Fig. 6D) and $F_{F2RU}–F_{F2RT}$ (Fig. 6C). The respective values are 3.4 and 7.6, indicating that MAP sensitivity was comparable or better than the sensitivity of impedance measurement for detecting the repressive effect of *F2R*-2.

F2R sgRNA suppresses thrombin-induced hyperpermeability

All the gene-targeting sgRNAs tested above repress, albeit to varying degrees, the expression of their target genes. Therefore, we gauged the combined effect of these sgRNAs on MAP permeability by comparing the sorting outcomes of a mixed population made up of equal-sized groups of MAPs carrying cells that express on each MAP one of the 15 sgRNAs employed in the study (five each for *F2R*, *GNAQ*, and *KDR*) to the sorting outcome of MAPs carrying cells that express neither sgRNAs nor dCas9-KRAB, similar to those shown in Appendix SI, Fig. S1D. The sorting outcome of the first group (Fig. 6E) shows that sgRNA expression almost abolished the population of untreated positive MAPs and reversed the distribution of thrombin-treated MAPs. The former was more than halved, and the latter increased by close to seven-fold. These large effects demonstrate the repressive efficacy of each gene-specific sgRNAs group. To visualize the individual effect of the most repressive *F2R*, *GNAQ* and *KDR*-targeted sgRNAs in comparison to three validated NC sgRNAs [8] on MAP permeability, we imaged the fluorescence of thrombin-treated MAPs with each of these sgRNAs. Cells expressing either *GNAQ*, or *KDR*-targeted sgRNAs responded to thrombin similarly to the negative-control sgRNA-expressing microcarriers (Fig. 6F). In contrast, the response of MAPs with cells that expressed the most effective *F2R* sgRNA was similar to that of MAPs carrying untreated cells that expressed one of the negative-control sgRNAs (top row of images in Fig. 6F). These results are consistent with the rest of the functional effects of the sgRNAs. The persistence of low fluorescence intensity emitted by MAPs carrying cell that express a *F2R* sgRNA indicates that thrombin treatment did not cause an artifactual signal resulting from cell detachment from the microcarrier surface. Nevertheless, since the sorting is to be used in combination with an inhibitory library, it needs to separate the microcarriers that emit the lowest light signal. Therefore, artifactually bright microcarriers cannot cause false gene identification.

DISCUSSION

In contrast to most if not all genetic screens performed to date, the new assay facilitates genetic screens of a collective cell function. Previous screens measured phenotypes that reflect changes in cell number, an activity of individual cells. Permeability is not amenable to existing functional assays, because it is inherently a collective cell function. The new assay repurposes a pre-existing device – microcarriers that had been developed over fifty years ago to increase

the surface available for the growth of adherent cells [51]. Microcarriers had already been used, in fact, to measure EC monolayer permeability, albeit in bulk format [35]. In contrast, the new assay deploys each cell-coated microcarrier as a single sample, thus taking advantage of the small microcarrier diameter of 150 μm on the average, to pack as many as 6000 microcarriers per mL of medium. At this sample concentration, 166 mL of growth medium would contain 10^6 microcarriers. As estimated above, this is a sufficiently large number of samples for performing a genome-wide screen with this functional assay.

Screens based on cell growth can measure a continuum of quantitative phenotypes by counting the numbers of cells that express sgRNAs of interest [52]. These measurements can be used for further analysis of the targets identified in the first screen, such as construction of genetic interaction (GI) maps [53]. Though the phenotypes of the MAPs (i.e., their fluorescence intensities), also vary continuously within a certain range, the sorting converts that range into an either “positive” or “negative” binary output, precluding the attribution of a continuous range of quantitative phenotypes to each sample, and of further analysis. This drawback can be overcome, however, by performing a set of replicate assays where the position of the gate is changed incrementally so that a larger range of phenotypes is sampled. Replicating the assay is straightforward because it can be run in as little as 30 min using a volume of less than 200 mL microcarriers in growth medium.

In addition to compactness, the format of the assay facilitates physical separation between samples that are either responsive or refractory to the stimulus, by using the phenotype as a sorting input. The separation is crucial for the identification of the genes that produce the measured phenotype. Counting the number of cells on the microcarriers, and determining if the cell monolayer reached confluence are straightforward because the cells on the microcarrier surface can be readily visualized by a dye and by other imaging modalities [35, 42]. The visibility enables growth of a clonal cell population from a single cell per microcarrier and makes it possible to verify that the cell monolayer coating the MAPs is confluent, preventing spurious signal as a result of probe binding to the exposed surface of the microcarrier. The duration of the assay, i.e. the time necessary for eliciting a measurable phenotype depends on the nature of the agonist, but it is not likely to allow sufficient time for the emergence of multiple phenotypes, such as change in cell density. This narrows the scope of the assay to its intended purpose of measuring intercellular permeability and prevents interference from other potential effects of the agonists which are often pleiotropic, such as VEGF. While the assay was validated by thrombin-induced hyperpermeability of EC monolayers, it is compatible with any monolayer-forming cell type, such as epithelial cells, and with any agonist that induces disruption of intercellular junctions.

Screening an untreated cell population that expresses a CRISPRi library would be potentially productive beyond its use for the removal of MAPs that carry non-confluent TIME cell monolayers. It is conceivable that the homeostasis of intercellular junctions requires the activity and turnover of certain proteins. At least some of the non-confluent microcarriers may carry clonal cell populations that express sgRNAs which knockdown genes that encode these proteins. Their identification could be as significant as that of genes that encode proteins which are required for the response to junction-disrupting agonists.

MATERIALS AND METHODS

Endothelial cell culture

TIME cells (American Type Cell Culture) were grown at 37°C in a humidified 5 percent CO_2 incubator in Vascular Cell Basal Medium supplemented with Microvascular Endothelial growth Kit-VEGF (American Type Cell Culture) and 12.5 µg/mL blasticidin (ThermoFisher Scientific).

Immunofluorescence

TIME cells grown to confluence on gelatin-coated round 12-mm glass coverslips (GG-12-Gelatin, Neuvitro) were treated with 2 U/mL thrombin (human α-thrombin, Enzyme Research Laboratories) for 30 min at 37°C, and 5 percent CO_2, or with PBS as a negative control. After washing in ice-cold PBS, fixation in 4 percent paraformaldehyde/PBS for 30 min at 23°C, and permeabilization in 0.1 percent Triton X-100 (Sigma-Aldrich) in PBS for 5 min, cells were incubated in a blocking solution of 5 percent BSA (Sigma-Aldrich) in PBS for 1 h. Immunolabeling by primary antibodies diluted according to the manufacturer's instructions in 0.1 percent Triton X-100 and1 percent BSA in PBS overnight at 4 °C was followed by a 3×PBS wash and incubation with 2.5 µg/mL fluorescently-conjugated secondary antibodies in PBS for 30 min at 23°C. After a 3×PBS wash, coverslips were mounted on glass slides (ProLong Gold Antifade Mountant, ThermoFisher Scientific). Images of TIME cells grown either as a two-dimensional culture or on microcarriers were acquired by epi-fluorescence microscopy (EVOS FL Auto Cell Imaging System, ThermoFisher Scientific).

Immunoblotting

Cells were scraped off plates, extracted in RIPA lysis buffer (25 mM Tris-HCl pH 7.6, 150mM NaCl, 1 percent NP-40, 1 percent sodium deoxycholate, 0.1 percent SDS; ThermoFisher Scientific) supplemented with phosphatase (Fisher Scientific) and protease (Sigma-Aldrich) inhibitor cocktails, and clarified by centrifugation (20,000 g, 10 min). Total protein concentration was determined by the BCA protein assay (ThermoFisher Scientific). Equal amounts of total protein were separated by 10 percent SDS-PAGE and transferred to a PVDF membrane. Membranes were blocked by 5 percent casein in TBS with 0.1 percent Tween 20, probed with the indicated primary antibodies, and incubated with HRP-conjugated secondary antibodies for 1 h at 23°C. Protein-antibody complexes were visualized by chemiluminescence (SuperSignal™ West Pico PLUS, ThermoFisher Scientific) on film (HyBlot CL® Autoradiography Film, Denville Scientific Inc.) or imaged by a charge-coupled device camera (Chemidoc Imaging System, BioRad).

Impedance measurement

Impedance was measured on xCELLigence Real-Time Cell Analyzer (ACEA Biosciences) according to the manufacturer's instructions. Briefly, 30000 TIME cells were seeded in 200 µL growth medium per well of an electronic 16-well plate (E-Plate View 16, ACEA Biosciences) for 30 min at 23°C to allow cell sedimentation. The cells were grown to confluence at 37°C, 5 percent CO_2. On the day of experiment, cells were treated by thrombin or by the same volume of carrier (PBS), and placed in the analyzer for continuous recording of impedance are needed. Relative impedance is expressed as $(Z_i-Z_0)/15\ \Omega$, where Z_i is the impedance at the i^{th} time point, and Z_0 is the initial impedance before the addition of thrombin.

Macromolecular permeability

TIME cells seeded at 1×10^5 per filter insert (0.4 µm pores, 6.4 mm diameter, polyethylene terephthalate membrane, Transwell®, Corning) were grown for 72 h in 24-well plates (Transwell®, Corning) filled with 800 µL growth medium per well. The cells in the inserts were

supplemented at the same time by either 2 U/mL thrombin or carrier, and by 1 μg/mL fluorescein isothiocyanate (FITC)-dextran (2000 kDa, Sigma-Aldrich) was added in the upper chamber. Ten μL samples were removed after 0, 5, 15, 30, 60, 90 and 120 min from the lower compartment, diluted in 90 μL of PBS, transferred in a 96 well black plate, clear bottom. Fluorescence in each well was measured with excitation at 485 nm and readout at 535 nm (VICTOR2, PerkinElmer). The results are expressed as light intensity counts.

TIME cell culture on microcarriers in spinner flasks

Cytodex 3 microcarriers (GE Health Sciences) were hydrated in a PBS volume of 50 mL/g for 3 h at 23°C, washed twice in a PBS volume of 30 mL/g, and autoclaved (121°C, 20 min). A quantity of 92 mg Cytodex 3 microcarriers were readied for cell growth by incubation overnight at 37°C, 5 percent CO_2, and stirred at 35 rpm (Troemner) in 50 mL growth medium in 100 mL siliconized (Sigmacote, Sigma-Aldrich) spinner flasks (Bellco Glass, model 1965-95010) equipped with a glass-ball plunger. TIME cells grown to 80 percent confluence in T75 flasks were briefly detached with 0.05 percent trypsin, 0.02 percent EDTA (American Type Cell Culture). The cells were then resuspended in growth medium supplemented with 15 percent FBS and 4.5 g/L glucose (supplemented growth medium). Microcarriers were inoculated with $6X10^6$ cells in 50 mL of supplemented growth medium to achieve a density of 24000 cells/cm^2. The microcarrier culture was incubated at 37°C, 5 percent CO_2 and stirred intermittently at 35 rpm for 1 min once every 15 min for a total of 1 hour, then stirred continuously at the same speed. Medium was replenished once every two days. Cells reached confluence in 3-5 days. In order to seed a single cell per microcarrier, the above amount of microcarriers was inoculated with $1.5X10^5$ cells to achieve a density of 600 cells/cm^2. To monitor cell growth on microcarriers, a small microcarrier sample was removed every day, treated with 2 μM of Calcein AM (ThermoFisher Scientific), and visualized by epifluorescence microscopy. Under these conditions, cells reached confluence in 9 days.

Detection of barrier disruption by fluorophore-conjugated fragment of fibronectin

To detect disruption of the confluent TIME cell monolayer on microcarriers, we used a 45 kDa FN_c (Sigma-Aldrich) purified from human plasma (Sigma-Aldrich) conjugated to Dylight 550 with a labeling kit (ThermoFisher Scientific). The cells were grown to confluence on gelatin-coated round 12-mm diameter glass coverslips (GG-12-Gelatin, Neuvitro). On the day of the permeability assay, the cells were treated with thrombin for 30 min at 2 U/mL and with 1 μg/mL Dylight 550-conjugated FN_{cf} for 5 min. The cells were then washed with ice cold PBS, fixed in 4 percent paraformaldehyde/PBS for 30 min, and washed again with PBS. The coverslips were mounted on glass slides with Prolong Gold (Invitrogen), a DAPI-containing medium. Permeability was characterized by quantifying dye fluorescence (DyLight 550, Ex/Em 562/576 nm, ThermoFisher Scientific) in epifluorescence images (EVOS FL, ThermoFisher Scientific).

Permeability in response to thrombin on cytodex3 microcarriers

TIME cells grown to confluence on microcarriers were incubated with 2 U/mL of Thrombin for 25 min in spinner flasks spun at 35 rpm at 37°C, 5 percent CO_2. The medium was then supplemented with 1 μg/mL FN_{cf} and stirred for 5 min. MAPs were transferred into a plate for visualization and quantification of the Dylight 550 dye by epifluorescence (EVOS FL).

Microcarrier sorting

MAPs treated as desired were fixed in 50 percent EtOH/PBS and 1 percent FBS for 10 min at 23°C, washed twice in PBS for 10 min at 4°C, and transferred to PBS with 1 percent FBS. MAPs were sorted at 561 nm on a Biosorter instrument (Union Biometrica) equipped with a FP-1000 1000 μm nozzle.

Expression of *dCas9-KRAB* and repressive sgRNAs in TIME cells and genomic DNA sequencing

Lentiviri were produced and infected into TIME cells as described [54]. The cells were transduced first by lentivirus expressing dCas9 fused to the KRAB repressor module [9] (pHR-SFFV-dCas9-BFP-KRAB, Addgene). Lentivirus-expressing cells were sorted (FACSAria II, BD Biosciences) using blue fluorescent protein (BFP) as a marker. Oligonucleotides encoding five optimized sgRNAs targeting the transcription start sites of *F2R*, *GNAQ*, and *KDR*, and NC sgRNAs were synthesized based on sequences from the CRISPRi V2 library designed by Horlbeck et al.[8]. Each sgRNA was subcloned into the backbone plasmid of the CRISPRi V2 library (pU6-sgRNA EF1Alpha-puro-T2A-BFP, Addgene) between the BstXI and BlpI restriction sites. Groups of *dCas9-KRAB*-expressing TIME cells were each infected separately by lentiviri expressing a single sgRNA and selected by puromycin resistance conferred by the sgRNA-expressing plasmid. sgRNA sequences are provided in Appendix SI, Table S1.

Statistics

The significance of the difference between means was determined by two-tailed Student's *t*-test. The null hypothesis was considered untrue if the probability satisfied the condition $P \leq 0.05$.

Non-standard Abbreviations

BFP – blue fluorescent protein
CRISPRa/i – activating or inhibitory clustered regularly interspaced short palindromic repeats sgRNA library
dCas9 – deactivated CRISPR-associated protein 9
EC – endothelial cell
FITC – fluorescein isothiocyanate
FNc – collagen-binding fragment of fibronectin
FNcf – fluorophore-conjugated FNc
KRAB – Krüppel-associated box (KRAB)
MAP – microcarrier assay of permeability
PAR – proteinase-activated receptor
qRT-PCR – quantitative real-time polymerase chain reaction
sgRNA – single guide RNA
TIME – telomerase-immortalized human dermal microvascular
UT – untreated
VE – vascular endothelial
VEGF – vascular endothelial growth factor
VP64 – tetrameric VP16 transactivation domai

DECLARATIONS

Ethics approval and consent to participate

No animals and no humans participated in this study.

Consent for publication

All authors consented for the publication of this study.

Availability of data and material

All data and materials generated in this study will be made available to the scientific community.

Competing Interests

The authors have no competing financial or other interests.

Funding
This study was supported by the National Heart Lung and Blood Institute (R01 grant HL119984 to AH and R01 grant HL128234 to LE) and by the National Cancer Institute (P30 grant CA56036 to PF).

Author Contributions
CS designed and performed experiments, analyzed the results, and wrote the manuscript; JY and XK performed experiments, analyzed the results, and prepared reagents; RK performed experiments, LE supervised the preparation of reagents and designed experiments; PF supervised the preparation of reagents and DNA sequencing, and analyzed data; EL designed experiments, analyzed data, and wrote the manuscript; AH conceived the study, coordinated its performance, designed experiments, analyzed the results, and wrote the manuscript.

Acknowledgments
We thank Dr. Florin Tuluc, Flow Cytometry Core Laboratory of the Children's Hospital of Philadelphia, for assistance in FACS; Drs. Luke Gilbert and Max Horlbeck, and by Ryan Pak, for assistance in the use of the CRISPR/dCas9 library developed in the lab of Dr. Jonathan Weissman, University of California, San Francisco. We thank Dr. Jonathan Weissman for depositing the CRISPRi library and dCas9-KRAB plasmid at Addgene.

REFERENCES

[1] Qi LS, Larson MH, Gilbert LA, Doudna JA, Weissman JS, Arkin AP, et al. Repurposing CRISPR as an RNA-guided platform for sequence-specific control of gene expression. Cell. 2013;152:1173-83.
[2] Shi J, Wang E, Milazzo JP, Wang Z, Kinney JB, Vakoc CR. Discovery of cancer drug targets by CRISPR-Cas9 screening of protein domains. Nat Biotechnol. 2015;33:661-7.
[3] Adamson B, Norman TM, Jost M, Cho MY, Nunez JK, Chen Y, et al. A Multiplexed Single-Cell CRISPR Screening Platform Enables Systematic Dissection of the Unfolded Protein Response. Cell. 2016;167:1867-82 e21.
[4] Manguso RT, Pope HW, Zimmer MD, Brown FD, Yates KB, Miller BC, et al. In vivo CRISPR screening identifies Ptpn2 as a cancer immunotherapy target. Nature. 2017;547:413-8.
[5] Konermann S, Brigham MD, Trevino AE, Joung J, Abudayyeh OO, Barcena C, et al. Genome-scale transcriptional activation by an engineered CRISPR-Cas9 complex. Nature. 2015;517:583-8.
[6] Chavez A, Tuttle M, Pruitt BW, Ewen-Campen B, Chari R, Ter-Ovanesyan D, et al. Comparison of Cas9 activators in multiple species. Nat Methods. 2016;13:563-7.
[7] Gilbert LA, Larson MH, Morsut L, Liu Z, Brar GA, Torres SE, et al. CRISPR-mediated modular RNA-guided regulation of transcription in eukaryotes. Cell. 2013;154:442-51.
[8] Horlbeck MA, Gilbert LA, Villalta JE, Adamson B, Pak RA, Chen Y, et al. Compact and highly active next-generation libraries for CRISPR-mediated gene repression and activation. Elife. 2016;5.
[9] Gilbert LA, Horlbeck MA, Adamson B, Villalta JE, Chen Y, Whitehead EH, et al. Genome-Scale CRISPR-Mediated Control of Gene Repression and Activation. Cell. 2014;159:647-61.
[10] Chen S, Sanjana NE, Zheng K, Shalem O, Lee K, Shi X, et al. Genome-wide CRISPR screen in a mouse model of tumor growth and metastasis. Cell. 2015;160:1246-60.
[11] Gayle S, Landrette S, Beeharry N, Conrad C, Hernandez M, Beckett P, et al. Identification of apilimod as a first-in-class PIKfyve kinase inhibitor for treatment of B-cell non-Hodgkin lymphoma. Blood. 2017;129:1768-78.
[12] Kurata M, Rathe SK, Bailey NJ, Aumann NK, Jones JM, Veldhuijzen GW, et al. Using genome-wide CRISPR library screening with library resistant DCK to find new sources of Ara-C drug resistance in AML. Sci Rep. 2016;6:36199.
[13] Tao L, Zhang J, Meraner P, Tovaglieri A, Wu X, Gerhard R, et al. Frizzled proteins are colonic epithelial receptors for C. difficile toxin B. Nature. 2016;538:350-5.
[14] Yamauchi T, Masuda T, Canver MC, Seiler M, Semba Y, Shboul M, et al. Genome-wide CRISPR-Cas9 Screen Identifies Leukemia-Specific Dependence on a Pre-mRNA Metabolic Pathway Regulated by DCPS. Cancer Cell. 2018.
[15] Napier BA, Brubaker SW, Sweeney TE, Monette P, Rothmeier GH, Gertsvolf NA, et al. Complement pathway amplifies caspase-11-dependent cell death and endotoxin-induced sepsis severity. J Exp Med. 2016;213:2365-82.
[16] Parnas O, Jovanovic M, Eisenhaure TM, Herbst RH, Dixit A, Ye CJ, et al. A Genome-wide CRISPR Screen in Primary Immune Cells to Dissect Regulatory Networks. Cell. 2015;162:675-86.
[17] Shi J, Zhao Y, Wang K, Shi X, Wang Y, Huang H, et al. Cleavage of GSDMD by inflammatory caspases determines pyroptotic cell death. Nature. 2015;526:660-5.
[18] Zimmermann S, Pfannkuch L, Al-Zeer MA, Bartfeld S, Koch M, Liu J, et al. ALPK1- and TIFA-Dependent Innate Immune Response Triggered by the Helicobacter pylori Type IV Secretion System. Cell Rep. 2017;20:2384-95.
[19] Burr ML, Sparbier CE, Chan YC, Williamson JC, Woods K, Beavis PA, et al. CMTM6 maintains the expression of PD-L1 and regulates anti-tumour immunity. Nature. 2017;549:101-5.

[20] Fei T, Chen Y, Xiao T, Li W, Cato L, Zhang P, et al. Genome-wide CRISPR screen identifies HNRNPL as a prostate cancer dependency regulating RNA splicing. Proc Natl Acad Sci U S A. 2017;114:E5207-E15.
[21] Wang T, Birsoy K, Hughes NW, Krupczak KM, Post Y, Wei JJ, et al. Identification and characterization of essential genes in the human genome. Science. 2015;350:1096-101.
[22] Xu C, Qi X, Du X, Zou H, Gao F, Feng T, et al. piggyBac mediates efficient in vivo CRISPR library screening for tumorigenesis in mice. Proc Natl Acad Sci U S A. 2017;114:722-7.
[23] Liu Y, Yu C, Daley TP, Wang F, Cao WS, Bhate S, et al. CRISPR Activation Screens Systematically Identify Factors that Drive Neuronal Fate and Reprogramming. Cell Stem Cell. 2018;23:758-71 e8.
[24] Stoletov K, Willetts L, Paproski RJ, Bond DJ, Raha S, Jovel J, et al. Quantitative in vivo whole genome motility screen reveals novel therapeutic targets to block cancer metastasis. Nat Commun. 2018;9:2343.
[25] Zhou P, She Y, Dong N, Li P, He H, Borio A, et al. Alpha-kinase 1 is a cytosolic innate immune receptor for bacterial ADP-heptose. Nature. 2018;561:122-6.
[26] Cong L, Ran FA, Cox D, Lin S, Barretto R, Habib N, et al. Multiplex genome engineering using CRISPR/Cas systems. Science. 2013;339:819-23.
[27] Erard N, Knott SRV, Hannon GJ. A CRISPR Resource for Individual, Combinatorial, or Multiplexed Gene Knockout. Mol Cell. 2017;67:348-54 e4.
[28] Aman J, van Bezu J, Damanafshan A, Huveneers S, Eringa EC, Vogel SM, et al. Effective treatment of edema and endothelial barrier dysfunction with imatinib. Circulation. 2012;126:2728-38.
[29] Kaneider NC, Leger AJ, Agarwal A, Nguyen N, Perides G, Derian C, et al. 'Role reversal' for the receptor PAR1 in sepsis-induced vascular damage. Nat Immunol. 2007;8:1303-12.
[30] Klei LR, Hu D, Panek R, Alfano DN, Bridwell RE, Bailey KM, et al. MALT1 Protease Activation Triggers Acute Disruption of Endothelial Barrier Integrity via CYLD Cleavage. Cell Rep. 2016;17:221-32.
[31] Fisher J, Linder A, Bentzer P, Boyd J, Kong HJ, Lee T, et al. Is Heparin-Binding Protein Inhibition a Mechanism of Albumin's Efficacy in Human Septic Shock? Crit Care Med. 2018;46:e364-e74.
[32] Rahbar E, Cardenas JC, Baimukanova G, Usadi B, Bruhn R, Pati S, et al. Endothelial glycocalyx shedding and vascular permeability in severely injured trauma patients. J Transl Med. 2015;13:117.
[33] Martin Y, Eldardiri M, Lawrence-Watt DJ, Sharpe JR. Microcarriers and their potential in tissue regeneration. Tissue Eng Part B Rev. 2011;17:71-80.
[34] Eaton BM, Toothill VJ, Davies HA, Pearson JD, Mann GE. Permeability of human venous endothelial cell monolayers perfused in microcarrier cultures: effects of flow rate, thrombin, and cytochalasin D. J Cell Physiol. 1991;149:88-99.
[35] Killackey JJ, Johnston MG, Movat HZ. Increased permeability of microcarrier-cultured endothelial monolayers in response to histamine and thrombin. A model for the in vitro study of increased vasopermeability. Am J Pathol. 1986;122:50-61.
[36] Park JH, Okayama N, Gute D, Krsmanovic A, Battarbee H, Alexander JS. Hypoxia/aglycemia increases endothelial permeability: role of second messengers and cytoskeleton. Am J Physiol. 1999;277:C1066-74.
[37] Waters CM. Flow-induced modulation of the permeability of endothelial cells cultured on microcarrier beads. J Cell Physiol. 1996;168:403-11.
[38] Owens RJ, Baralle FE. Mapping the collagen-binding site of human fibronectin by expression in Escherichia coli. EMBO J. 1986;5:2825-30.
[39] Engvall E, Ruoslahti E, Miller EJ. Affinity of fibronectin to collagens of different genetic types and to fibrinogen. J Exp Med. 1978;147:1584-95.

[40] Laposata M, Dovnarsky DK, Shin HS. Thrombin-induced gap formation in confluent endothelial cell monolayers in vitro. Blood. 1983;62:549-56.
[41] Rabiet MJ, Plantier JL, Rival Y, Genoux Y, Lampugnani MG, Dejana E. Thrombin-induced increase in endothelial permeability is associated with changes in cell-to-cell junction organization. Arterioscler Thromb Vasc Biol. 1996;16:488-96.
[42] Haselton FR, Mueller SN, Howell RE, Levine EM, Fishman AP. Chromatographic demonstration of reversible changes in endothelial permeability. J Appl Physiol (1985). 1989;67:2032-48.
[43] Van Itallie CM, Holmes J, Bridges A, Gookin JL, Coccaro MR, Proctor W, et al. The density of small tight junction pores varies among cell types and is increased by expression of claudin-2. J Cell Sci. 2008;121:298-305.
[44] Ebnet K, Schulz CU, Meyer Zu Brickwedde MK, Pendl GG, Vestweber D. Junctional adhesion molecule interacts with the PDZ domain-containing proteins AF-6 and ZO-1. J Biol Chem. 2000;275:27979-88.
[45] Ngok SP, Geyer R, Liu M, Kourtidis A, Agrawal S, Wu C, et al. VEGF and Angiopoietin-1 exert opposing effects on cell junctions by regulating the Rho GEF Syx. J Cell Biol. 2012;199:1103-15.
[46] Srinivasan M, Sedmak D, Jewell S. Effect of fixatives and tissue processing on the content and integrity of nucleic acids. Am J Pathol. 2002;161:1961-71.
[47] Kataoka H, Hamilton JR, McKemy DD, Camerer E, Zheng YW, Cheng A, et al. Protease-activated receptors 1 and 4 mediate thrombin signaling in endothelial cells. Blood. 2003;102:3224-31.
[48] Quinn TP, Peters KG, De Vries C, Ferrara N, Williams LT. Fetal liver kinase 1 is a receptor for vascular endothelial growth factor and is selectively expressed in vascular endothelium. Proc Natl Acad Sci U S A. 1993;90:7533-7.
[49] McLaughlin JN, Shen L, Holinstat M, Brooks JD, Dibenedetto E, Hamm HE. Functional selectivity of G protein signaling by agonist peptides and thrombin for the protease-activated receptor-1. J Biol Chem. 2005;280:25048-59.
[50] Bischoff I, Hornburger MC, Mayer BA, Beyerle A, Wegener J, Furst R. Pitfalls in assessing microvascular endothelial barrier function: impedance-based devices versus the classic macromolecular tracer assay. Sci Rep. 2016;6:23671.
[51] van Wezel AL. Growth of cell-strains and primary cells on micro-carriers in homogeneous culture. Nature. 1967;216:64-5.
[52] Kampmann M, Bassik MC, Weissman JS. Integrated platform for genome-wide screening and construction of high-density genetic interaction maps in mammalian cells. Proc Natl Acad Sci U S A. 2013;110:E2317-26.
[53] Bassik MC, Kampmann M, Lebbink RJ, Wang S, Hein MY, Poser I, et al. A systematic mammalian genetic interaction map reveals pathways underlying ricin susceptibility. Cell. 2013;152:909-22.
[54] Kampmann M, Bassik MC, Weissman JS. Functional genomics platform for pooled screening and generation of mammalian genetic interaction maps. Nat Protoc. 2014;9:1825-47.

FIGURE LEGENDS

Figure 1: Microcarriers are repurposed as miniature individual permeability assays. A. Gelatin-coated microcarriers composed of cross-linked dextran carry a confluent EC monolayer (green, to designate calcein-loaded ECs, as shown in Figs. 3 and 5), incubated in medium containing the collagen-binding proteolytic fragment of fibronectin conjugated to a fluorophore (FN_{cf}). Once treated by a junction-disrupting agonist (thrombin in this study), FN_{cf} binds to the exposed gelatin surface between cells whose junctions disassembled in response to the agonist. **B.** Microcarriers carrying untreated ECs bind a minimal amount of FN_{cf}. Microcarriers carrying agonist-treated ECs bind varying amounts of $FN_{cf,}$ depending on the identity of the gRNA expressed by the clonal cell population on each microcarrier. Microcarriers carrying ECs that express gRNAs targeting genes that encode proteins required for the induction of the disassembly of cell-cell junctions bind a low amount $FN_{cf,}$ similar to untreated microcarriers. ECs expressing gRNAs that are unrelated to the signaling pathway of the junction-disrupting agonist respond by disassembling their junctions. FN_{cf} binds to the gelatin surface exposed between the responsive ECs, rendering the microcarriers that carry these cells fluorescent. The fluorescent microcarriers and the dark microcarriers are separated by fluorescence assisted sorting. The gates of the sorting machine can be set up to capture any group of interest in this population, based on the fluorescence intensity of the microcarriers of interest.

Figure 2: Thrombin increases the paracellular permeability of TIME cell monolayers. A. The permeability of TIME cell confluent monolayers grown on filter inserts to 2000 kDa FITC-dextran increased in response to treatment by 2.0 U thrombin applied at t=0 min for the duration of the experiment, as indicated by the augmentation of the fluorescence signal from the bottom well under the filter. **B.** The impedance of TIME cell monolayers grown on electrodes embedded in the bottom of multi-well plates fell sharply after treatment by the indicated dosages of thrombin (applied as above), indicating that the integrity of the monolayer deteriorated. **C.** Epifluorescence images of confluent TIME cells in monolayers grown on gelatin-coated coverslips. Intercellular junctions disassembled upon treatment by 2 U/mL thrombin (Thr), as indicated by the change in the VEcad signal. The cells formed thicker stress fibers and detached from each other. Magnified images of the regions marked by squares are shown on the left and right sides. Scale bars, 50 μm.

Figure 3: TIME cells form a clonal confluent cobble-stone monolayer on microcarriers. A. Images of calcein AM-stained TIME cells seeded on microcarriers at a density of 1.5×10^4 cells/cm^2 microcarrier surface area and grown for the indicated durations in spinner flasks. The cells reached confluence after 4 days and formed a tightly-sealed monolayer (see cell junctions in inset). Scale bars, 200 (top row) and 100 (bottom row) μm. **B.** When initiated from a single TIME cell per microcarrier, a confluent monolayer was formed in 9 days. The inset visualizes intercellular junctions. Scale bar, 100 μm.

Figure 4. Binding of FN_{cf} removes non-confluent MAPs. A. Gallery of emission and extinction intensity profiles of individual MAPs. **B**. Density plot of MAP extinction per time-of-flight of the untreated MAP population that was incubated with FN_{cf} prior to sorting, and histogram showing the gate placed at approximately 2-fold intensity of the median peak of MAP fluorescence intensity. **C.** Density plot of the sorted MAP population and histogram showing MAP counts per their peak fluorescence intensities. **D.** Image of a group of presorted MAPs showing the fluorescence of bound FN_{cf}. **E.** A similar image of a group of sorted MAPs (scale bar, 1 mm).

Figure 5. Highly effective sgRNAs reduce substantially the expression and abundance of the targeted gene and encoded protein, respectively. A. Quantification of qRT-PCR measurements of the expression levels of *F2R* in TIME cells transduced by each one of the five CRISPRi library sgRNAs that target *F2R* (mean±SD, n=3). The immunoblot (one of duplicate experiments) on the right side shows PAR1 abundance in TIME cells transduced by the same sgRNAs. **B** and **C**. The same measurements as above for the sgRNAs that target *GNAQ* or *KDR*. **D.** Impedance traces of TIME cells expressing each of the indicated sgRNAs. Thrombin was applied to all the cell groups at the time point marked by an arrow, normalized relative to the impedance of untreated (UT) cells expressing negative control (NC-2) sgRNA.

Figure 6. *F2R* sgRNA suppresses thrombin-induced hyperpermeability. A. Time course of impedance measurements of thrombin-treated TIME cells normalized relative to the impedance of untreated (UT) cells expressing negative control (NC-2) sgRNA. **B.** Density plot of peak fluorescence of a presorted population of MAPs that carry cells transduced by *F2R*-targeting sgRNA showing the sorting gate; a histogram showing counts per peak fluorescence of the sorted MAPs gated in respect to the density plot; a quadruplet of individual MAP emission and extinction profiles. **C.** Histograms showing counts per peak fluorescence of sorted MAPs that carry cells transduced by *F2R*-targeting sgRNA, either untreated or treated by thrombin. **D.** Effects of thrombin treatment on the fluorescence intensity of MAPs carrying TIME cell transduced by the indicated sgRNAs. **E.** Percentages of MAPs sorted from a population consisting of equal numbers of MAPs of cells transduced by each of the18 sgRNAs employed in the study (five each for *F2R*, *GNAQ*, and *KDR*, and three negative-control sgRNAs) under the indicated conditions (mean±SD, n=4). **F.** Triplicate fluorescence images of the MAPs carrying cells transduced by the indicated sgRNAs, under the indicated conditions. Scale bar, 100 μm.

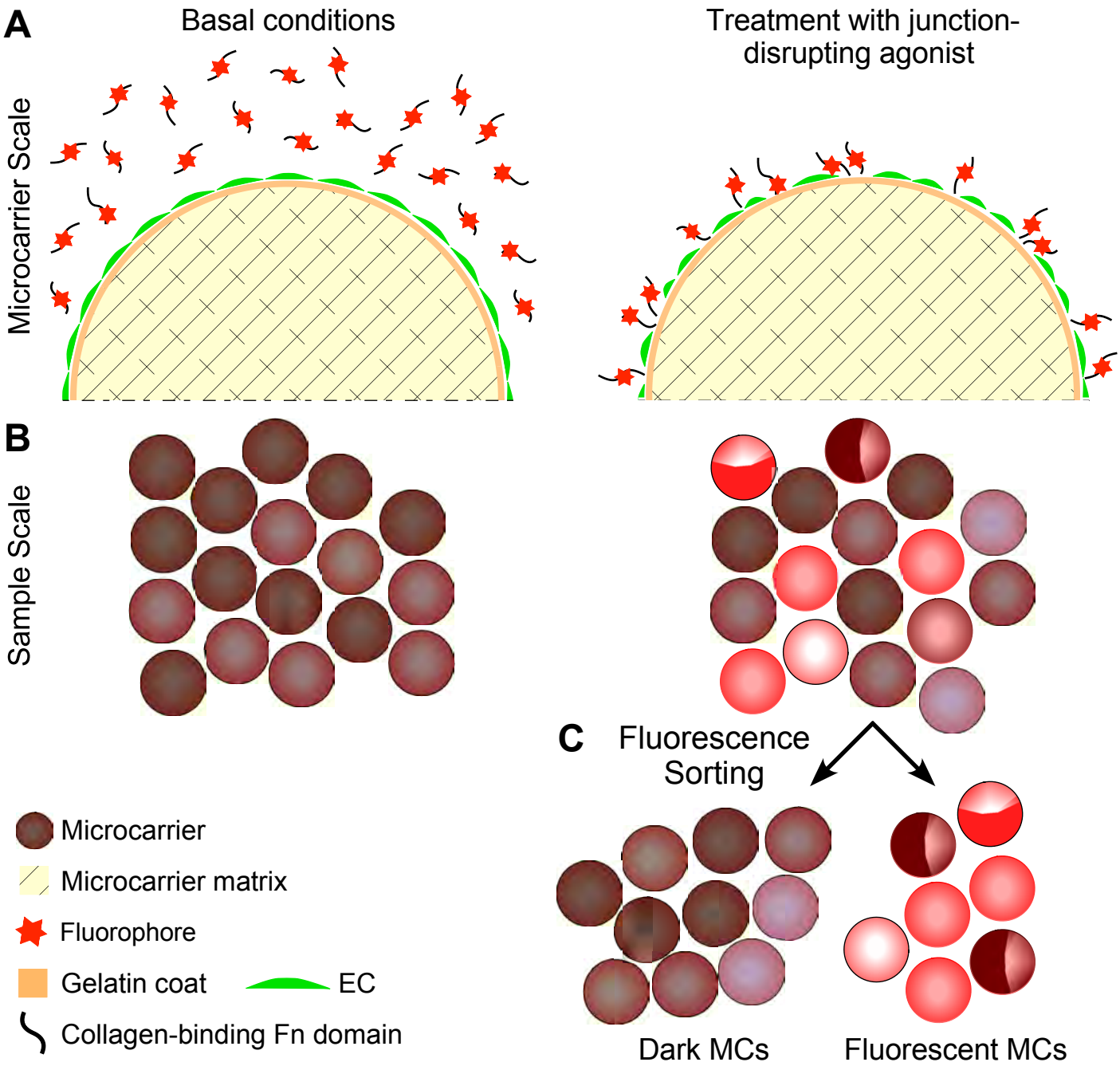

Figure 1

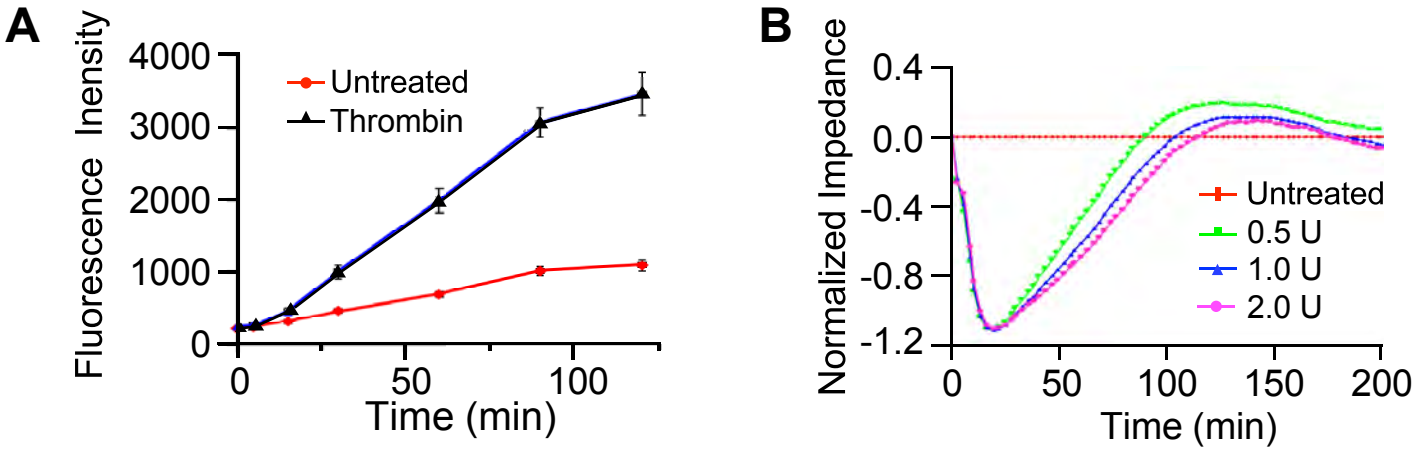

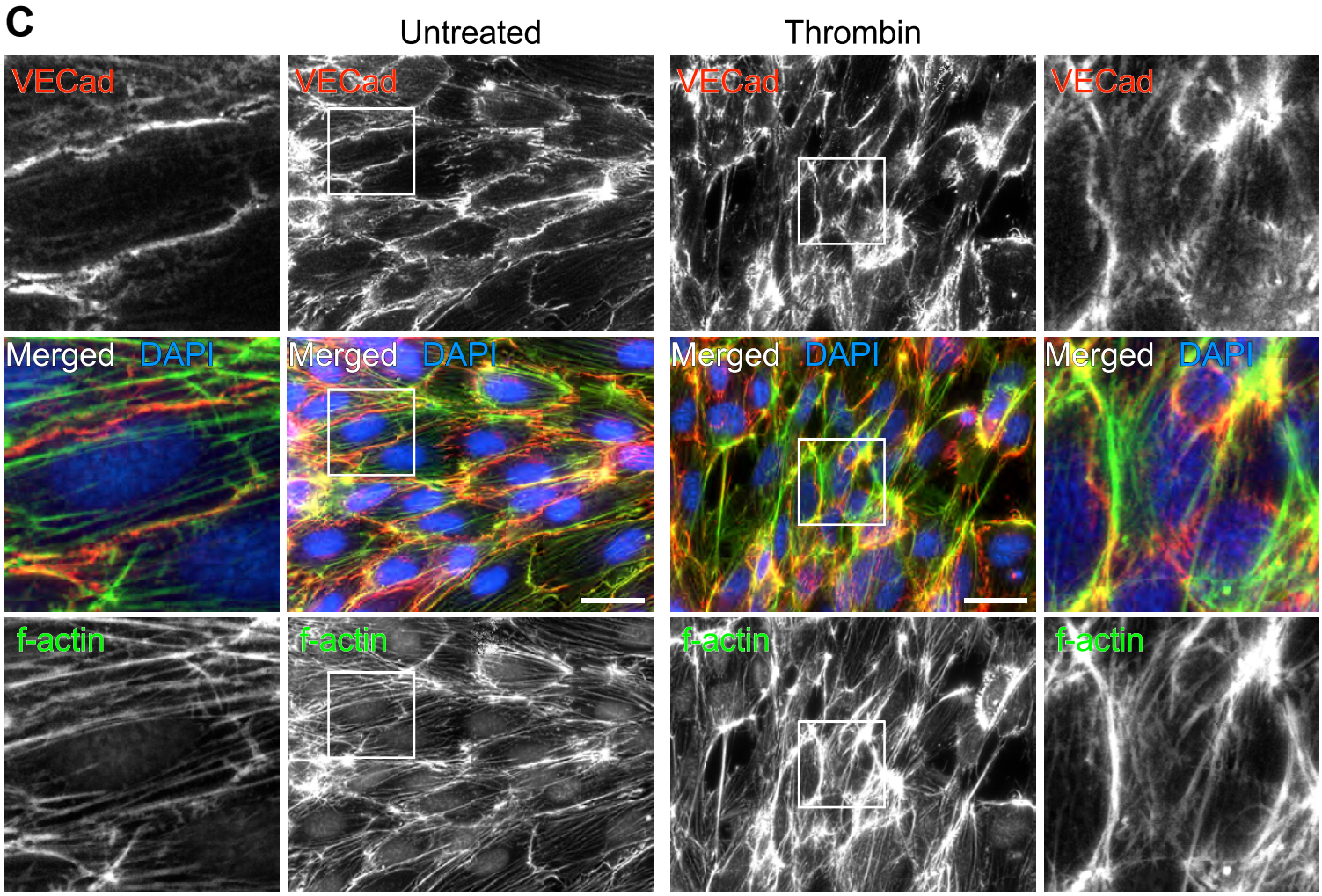

Figure 2

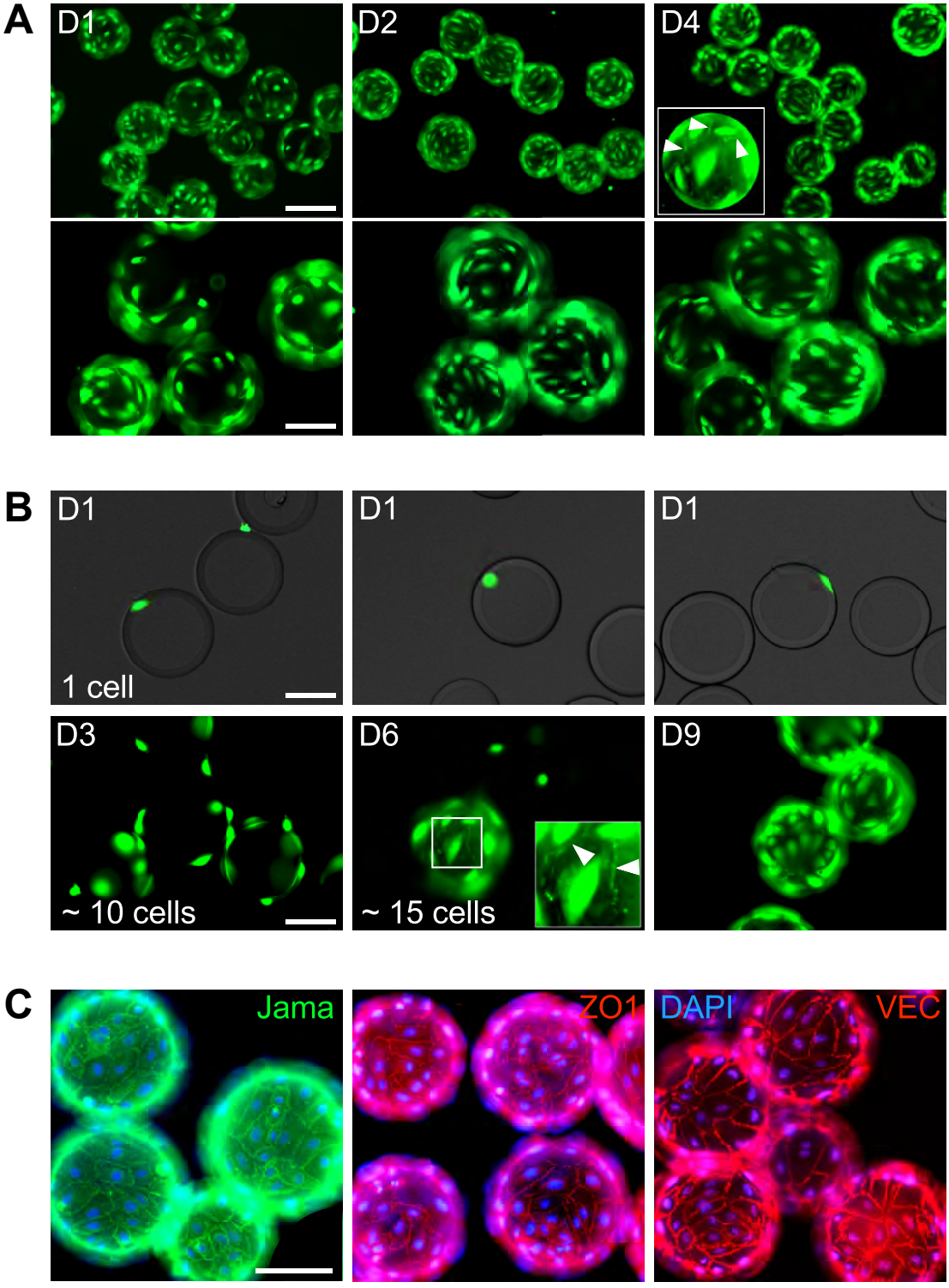

Figure 3

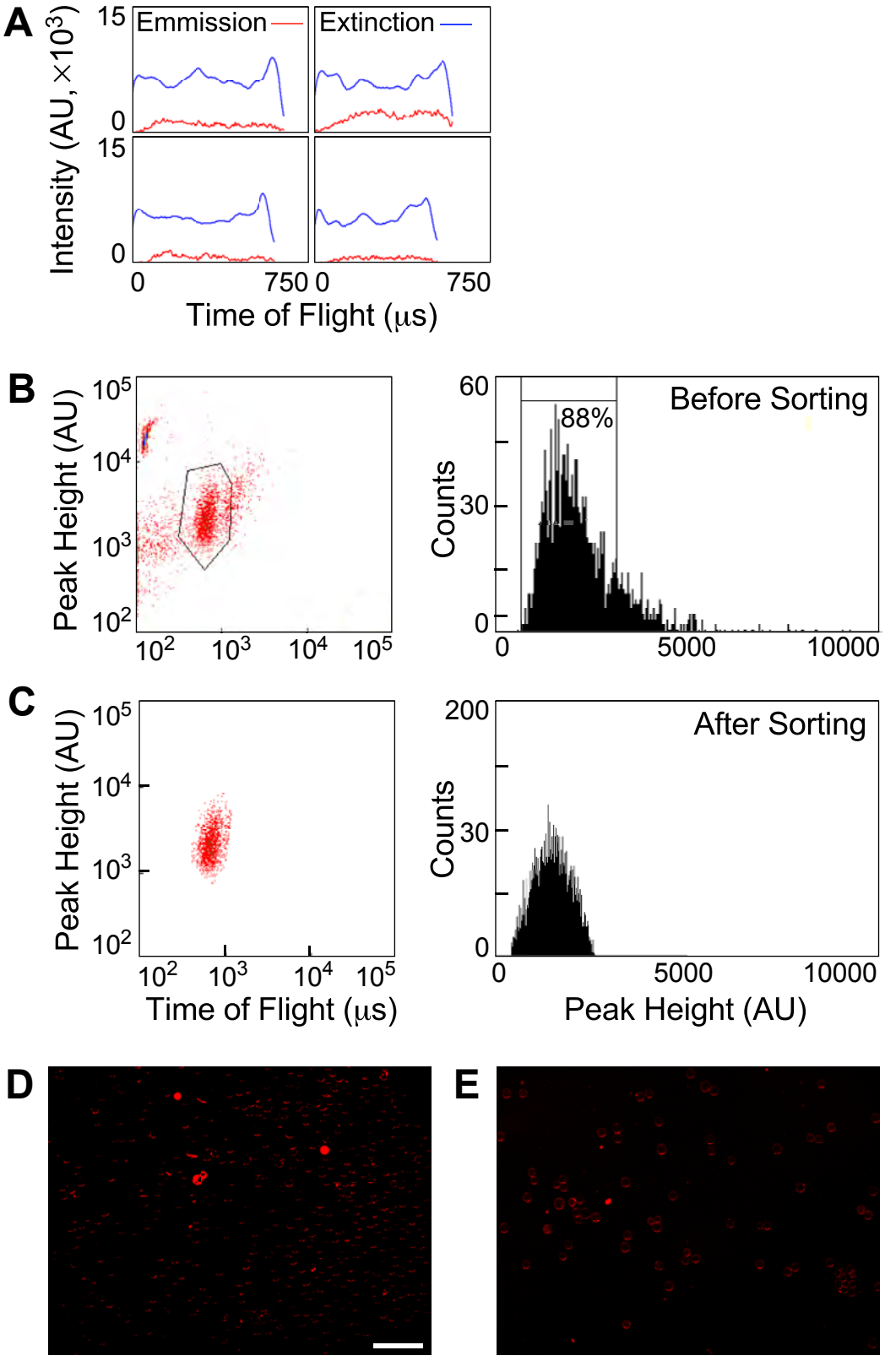

Figure 4

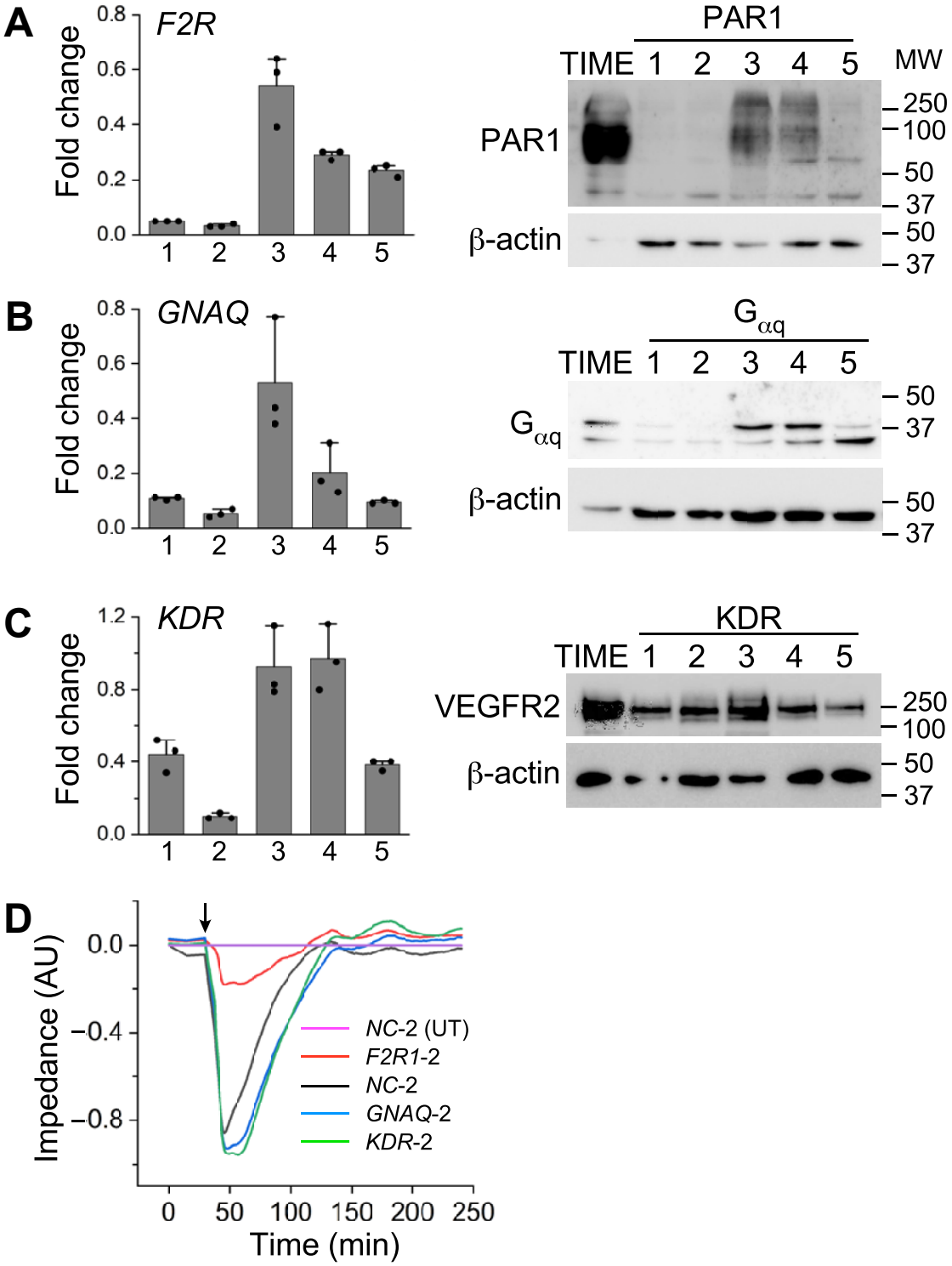

Figure 5

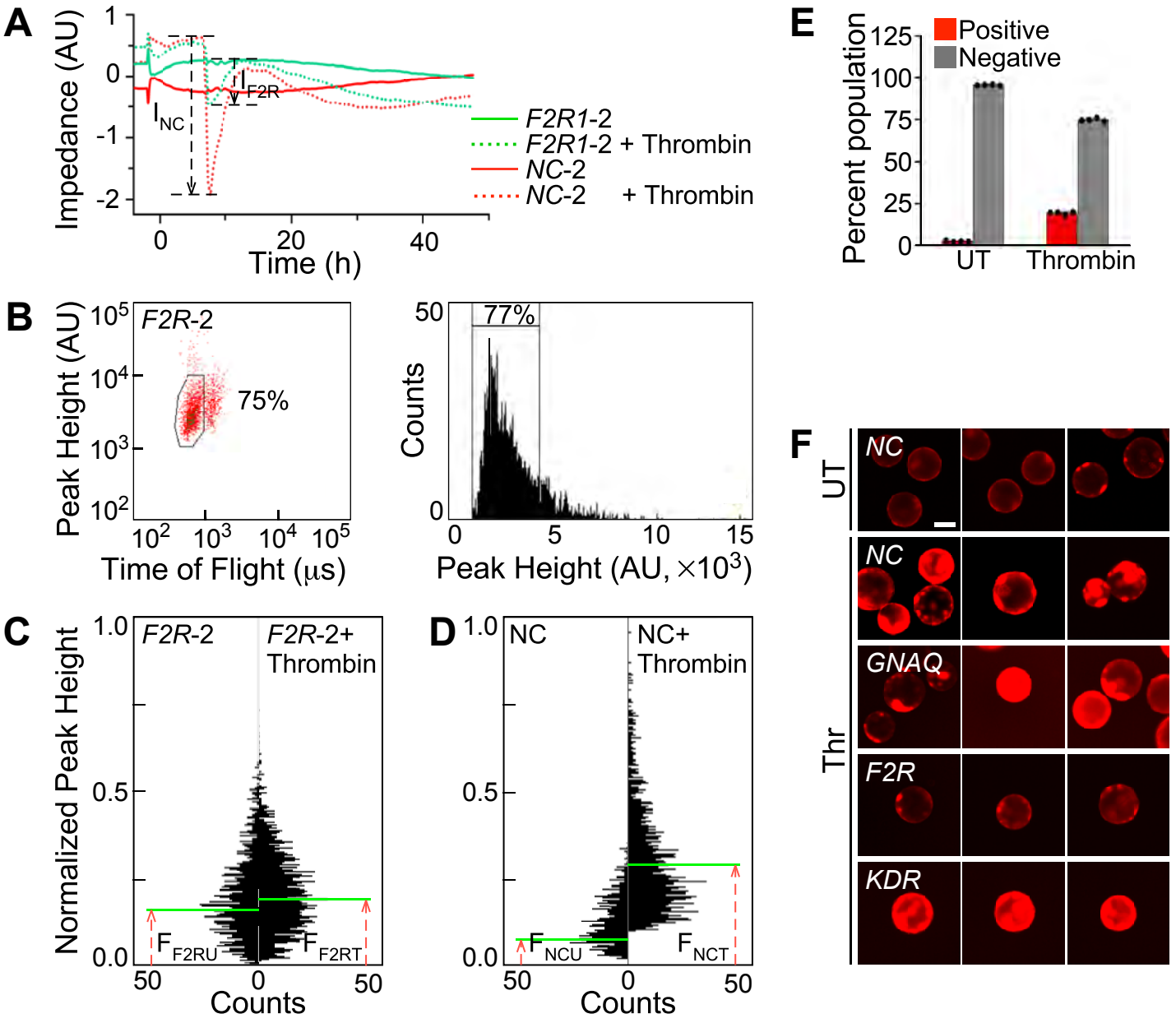

Figure 6